Korean J. Chem. Eng., 34(9), 2488-2497 (2017)
DOI: 10.1007/s11814-017-0125-y

pISSN: 0256-1115
eISSN: 1975-7220

Surface modification of silica-graphene nanohybrid as a novel stabilizer for oil-water emulsion

Sanaz Tajik*, Bahram Nasernejad*,†, and Alimorad Rashidi**

*Faculty of Chemical Engineering, Amirkabir University of Technology, Hafez Ave, P. O. Box 15875-4413, Tehran, Iran
**Nanotechnology Research Center, Research Institute of Petroleum Industry (RIPI), P. O. Box 14665-1998, Tehran, Iran
(*Received 15 February 2017 • accepted 1 May 2017*)

Abstract−The surface modification of silica-graphene nanohybrid through treatment with a mixture of nitric and sulfuric acid vapors to prepare a novel stabilizer for decalin-water emulsion was investigated. The nanohybrid was prepared through chemical vapor deposition using silica aerogel and acetylene as catalyst and carbon precursor at atmospheric pressure and 600 °C. The physicochemical properties of the modified nanohybrid were characterized by FT-IR, XPS, Raman spectroscopy, and TEM. The surface modification of nanohybrid was at various duration times (24, 48, and 72 hours) to optimize the surface modification conditions. Zeta potential of −39.9 mV revealed that the surface modification of nanohybrid after 72 hours had an excellent stability in aqueous phase due to the presence of exceptional functional groups. The emulsion average droplet size decreased by increasing the nanohybrid concentration. The negative value of the zeta potential showed the proposed nanohybrid can be applied as an appropriate stabilizer for emulsion.

Keywords: Chemical Vapor Deposition, Nanostructures, Functional Groups, Silica-graphene, Stabilizer

INTRODUCTION

Increasing the stability of oil-water emulsion plays a pivotal role in many industrial fields [1-5]. Although addition of surfactants as stabilizer agent has been diminished due to their high toxicity, corrosion, and environmental problems, anionic or cationic surfactants are still proposed to produce stable emulsions. Thus, elimination of hazardous surfactants and developing an alternative technique for increasing the stability of emulsion are the current challenges in this field. It has been reported that the use of solid nanoparticles for stabilization of emulsions helps to reduce the concentration of conventional emulsifying agents or even their complete elimination [6,7]. Up to now, Pickering emulsions have been identified as well-known two-phase oil-water emulsions that can be stabilized by using solid nanoparticles at the interface of oil-water through physical interactions [8]. Pickering emulsions can be stabilized by particles that are partly wetted by the two phases [9]; however, particles that are completely wetted by either water or oil are dispersed in that phase and a Pickering emulsion cannot be formed [6,10]. Although various kinds of organic and inorganic materials such as solid lipids, silica, carbon, titanium dioxide, and ferric oxide nanoparticles have been employed for the stabilization of oil-water Pickering emulsions [11-14], a few of these nanoparticles are able to form stable emulsions with a suitable size distribution and higher stability. In fact, the addition of nanoparticles replaces the liquid-liquid interfaces with solid-liquid interfaces which have a less interfacial energy [15]. As a new and efficient achievement, it has been proved that the nanoparticles would facilitate and increase the dispersion of immiscible droplets into the other liquids, leading to the stable and cost-effective emulsifiers [1,16].

Additionally, the control of some solid particles properties, including their concentration, shape, and size, plays an important role in Pickering emulsion behavior. The concentration of particles has been confirmed to be a key factor in Pickering emulsion properties [17]. The stability of Pickering emulsions is also affected markedly by the hydrophilic-lipophilic balance (HLB) of the particles that should be adjusted [18]. Consequently, although some types of organic and inorganic materials can produce stable Pickering emulsions, stabilization of emulsion with solid particles is still a major challenge [19].

Graphene and its derivatives as a new class of 2D materials have attracted attention in various fields from industrial [20,21] to biomedical applications [22-24]. Among the state-of-the-art nanoparticles, surface modified graphene has been recently used to produce stable Pickering emulsion due to their remarkable properties [25,26]. On the other hand, silica-based nanomaterials have been widely exploited as an encouraging nano additive for the preparation of stable Pickering emulsions, due to their exceptional characteristics such as unique morphology, size, porosity, and high affinity to various functional groups [27-29]. It has been recently suggested that the combination of graphene and silica-based materials can be used to produce solid-stabilized Pickering emulsions because of the synergetic effect of the nanohybrid versus bare graphene and silica powder. However, owing to the inertness of graphene sheets, which leads to a rapid aggregation in polar aqueous solution, development of a well-stabilized Pickering emulsion by the use of surface modified graphene has been shown an increasing interest.

Surface modification of hydrophobic graphene nanohybrids can

†To whom correspondence should be addressed.
E-mail: banana@aut.ac.ir

be employed as a suitable substitution of surfactants for stabilization of emulsions. The creation of oxygen containing functional groups such as carboxyl and hydroxyl at the edge or on the basal planes of graphene sheets [30] leads to boost the hydrophilicity of graphene nanohybrid due to the oxidation process [31]. Numerous methods such as ozonation [32], plasma enhancement [33], and acid treatment in liquid phase [34] were reported for oxidation and surface modification of carbon nanostructures. Most of the conventional methods are based on acidic treatment in liquid phase which suffer from disadvantages such as harsh synthesis condition, cumbersome separation or filtration, corrosive media, structural damages which require sophisticated devices [35,36]. Hence, gas phase surface modification of carbon nanostructures can be a proper alternative to overcome the above-mentioned issues. Xia et al. [37] have proposed the vapor phase surface modification by nitric acid for carbon nanotube that shows many advantages compared to liquid phase surface modification, especially the elimination of filtering step. Herein, silica-graphene nanohybrid was first synthesized through chemical vapor deposition technique (CVD) using silica powder as a heterogeneous catalyst without any additional step for removing catalyst. Afterwards, a desired proportion of sulfuric and nitric acid in gas phase was used for the surface modification of the silica-graphene nanohybrid. The proposed method facilitates the surface modification of silica-graphene nanohybrid through eliminating the difficult steps such as filtration, purifying, washing, and drying compared to other reported methods. Furthermore, addition of sulfuric acid might enhance the relative volatility of nitric acid, which is essential to accomplish a high level of modification. The time of surface modification was altered and optimized to get the highest level of oxygen containing functional groups on the silica-graphene nanohybrid. Finally, the effect of surface modification time and the concentration of nanohybrids on the emulsion droplet size were visually investigated by microscopy images. The as-prepared surface modified silica-graphene nanohybrid was used as a promising stabilizer for the preparation of stable decalin-water emulsion.

EXPERIMENTAL

1. Materials

All chemicals, including sulfuric acid (H_2SO_4, 98%), nitric acid (HNO_3, 65%), citric acid monohydrate, methanol, sodium silicate (Na_2SiO_3-specific gravity 1.05), and decahydronaphthalene (decalin, >98%), were purchased from Merck. Acetylene (C_2H_2), hydrogen (H_2), and nitrogen (N_2) gasses with a purification of 99.99% were from an Iranian gas corporation and distilled deionized water was used in all experiments.

2. Characterization

Powder X-ray diffraction (XRD) measurements were carried out on a Philips X'pert diffractometer, using filtered Cukα radiation (K=1.54 °A). Transmission electron microscopy (TEM) images were obtained with a field emission gun transmission electron microscope (Tecnai G2 F20 S-TWIN HR(S) TEM, FEI). The Raman spectra were acquired on a Jovin Yvon Horiba Lab Ram equipped with a charge-coupled detector and a He-Ne laser (632 nm) as excitation source. The X-ray photoelectron spectra were obtained by X-ray photoelectron spectroscopy (XPS, SPECS Germany, PHOIBOS 150). Fourier transform infrared spectroscopy (FTIR) was performed in the range of 400 cm^{-1} and 4,000 cm^{-1} (Tensor 27, Bruker Inc., Germany). Thermogravimetric analysis measurement was on a Shimadzu TG50 analyzer. Malvern Zetasizer Nano ZS was used for measuring zeta potential. A Nikon LV100D optical microscope was used to take images from the droplets.

3. Synthesis of Silica-graphene Nanohybrids

The silica aerogel was prepared by using a special sol-gel method [38]. The preliminary experiments were conducted at various temperatures, heating rates, time, flow rates, and concentrations of silica aerogel. In a typical experiment, the nanohybrids were achieved by annealing of 1 g silica aerogel powders in a horizontal quartz tube furnace under a flow of H_2 (600 sccm) up to 600 °C (heating rate of 5 °C/min). Afterwards, acetylene gas with the flow rate of 100 sccm was injected into the reaction for 30 min. Finally, the sample was immediately cooled to room temperature under N_2 atmosphere.

4. Surface Modification Method

The applied experimental set-up for surface modification of silica-graphene nanohybrid is shown in Fig. 1. It consists of a round bottom flask, a fixed bed reactor equipped with a heater, temperature controller, and a condenser. The tubular reactor was heated by a resistance heating coil. Surface modified silica-graphene nanohybrids were prepared through loading 0.1 g of nanohybrids into the reactor and heating to 100 °C. The round bottom flask was filled with 150 ml of a mixture of concentrated nitric and sulfuric acid (1 : 3 v/v) and heated to 150 °C, under magnetic stirring, in an ethylene glycol bath. The condenser was used to ensure that the surface modification process was completely accomplished at vapor phase without any contact with liquid acids. The ethylene glycol bath was turned off after the desired time (24, 48, and 72 h), while the reactor heater was kept on for 2 h to dry nanohybrids. Hereaf-

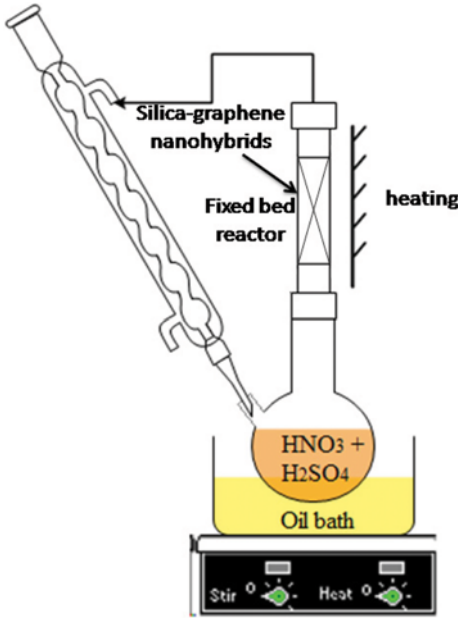

Fig. 1. Schematic illustration of the set-up used for silica-graphene nanohybrids treatment with acid vapor.

ter, the modified silica-graphene nanohybrids at 24, 48, and 72 h are denoted as fsg.24, fsg.48, and fsg.72, respectively.

5. Preparation of Pickering Emulsion with Pristine and Surface Modified Silica-graphene Nanohybrids

The oil-water emulsions were prepared by adding modified nanohybrids in the mixture of deionized water and decalin as the aqueous and organic phases, respectively. The preliminary experiments were conducted at the various ratios of water/decalin and the different amounts of nanohybrid. The ratio of (1 : 1 v : v) water/decalin was selected as the optimized proportion due to its higher stability. In a typical experiment, the nanohybrids were thoroughly dispersed in aqueous phase by sonication of 0.01, 0.05, and 0.1 (wt%) of nanohybrids (bath sonicator 100 W) for 30 minutes. Afterwards, decalin was added and the mixture was sonicated by an ultrasonic device with a dipping probe close to the surface at 60 W for 1 minute. Finally, the microscopic images were taken via dropping the as-prepared emulsion on microscopic glass slides.

RESULTS AND DISCUSSION

Fourier transform infrared spectroscopy (FT-IR) was used to characterize the as-prepared nanohybrids. According to the FT-IR spectra (Fig. 2), obvious differences between pristine and surface modified silica-graphene nanohybrids can be observed. However, there is not a distinguishable difference in the chemically modified nanohybrids spectra after 24, 48, and 72 h, indicating the creation of desired oxygen containing functional groups mostly in the first 24 h. Typical hydroxyl stretching absorption for C-OH and HO-C=O groups appeared at 2,700-3,500 cm^{-1} as a broad peak confirming a high degree of oxidation (lines b-d). The characteristic absorption signal corresponding to the C=O stretching band was also observed at 1,733.03 cm^{-1} (lines b-d). In all spectra, the absorption band for C=C (aromatics) can be seen around 1,636 cm^{-1} (lines a-d). In addition, the weak peak at around 1,384.39 cm^{-1} can be attributed to the C-O (carboxyl groups) stretching band.

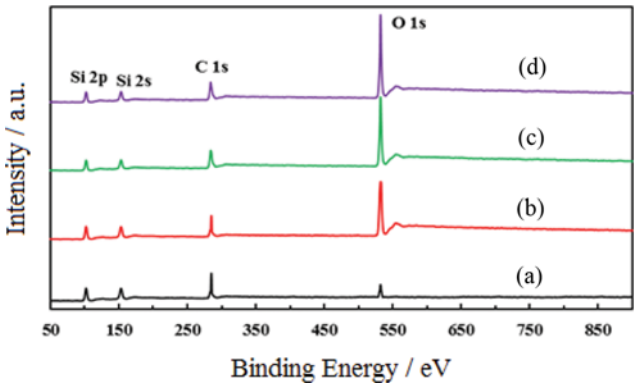

Fig. 3. X-ray photoelectron spectra of (a) silica-graphene nanohybrid, (b) fsg.24, (c) fsg.48, and (d) fsg.72.

The FT-IR spectra reveal that by increasing the surface modification time from 24 to 72 h, there is no distinct change regarding the functional groups. It shows that the surface of nanohybrid in the surface modification reaction has been considerably saturated during 24 h. However, the effect of this chemical modification time was thriving on the size of droplets as illustrated by microscopic images.

The X-ray photoelectron spectrum (XPS) was also used to further characterize the surface composition of the prepared silica-graphene and modified nanohybrids. Fig. 3 shows all pristine and modified silica-graphene nanohybrids composed of carbon, oxygen, and silica as the main elements, indicating the lack of any impurity. Fig. 4(a)-(d) represents the high resolution core level of C1s XPS spectra. As can be seen in Fig. 4(a)-(d), all C1s XPS spectra are fitted with four Gaussian peaks corresponding to C-C, C-O, C=O, and O=C-O binds. The values of carbon-to-oxygen (C/O) ratio of the samples were calculated and summarized in Table 1. The XPS results also demonstrate noticeable differences between pristine and surface modified silica-graphene nanohybrids. How-

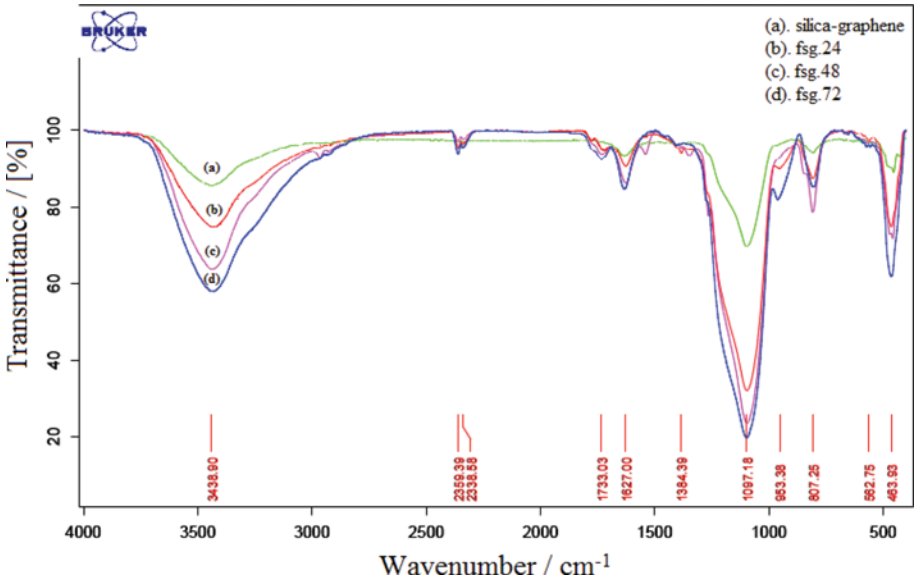

Fig. 2. The FT-IR spectra of the pristine silica-graphene nanohybrid (a) and surface modified at 24 (b), 48 (c), and 72 h (d).

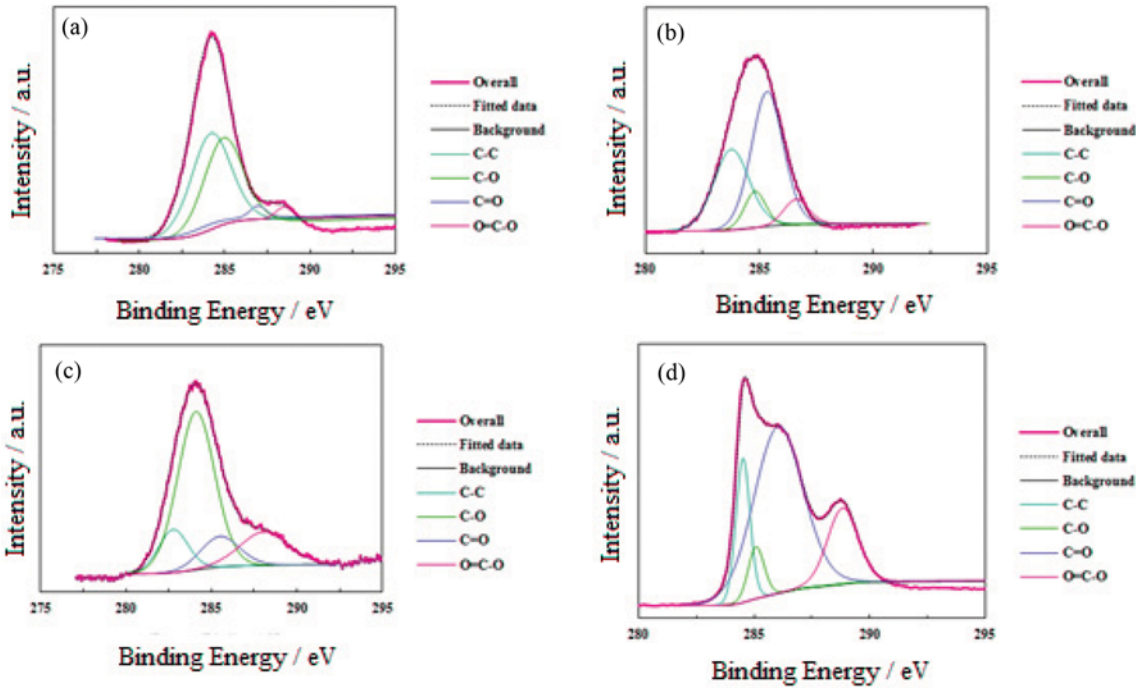

Fig. 4. High resolution XPS spectra of (a) Silica-graphene nanohybrid, (b) fsg.24, (c) fsg.48, and (d) fsg.72.

Table 1. Atomic concentration of the samples based on XPS

Sample	Concentration of carbon/atomic %	Concentration of oxygen/atomic %	C/O ratio
Silica-graphene nanohybrid	68.77	15.72	4.37
Fsg.24	36.89	39.78	0.93
Fsg.48	26.43	48.09	0.55
Fsg.72	21.96	54.69	0.40

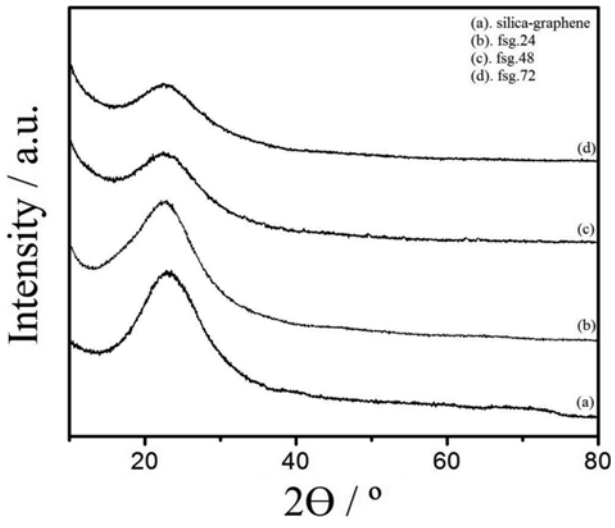

Fig. 5. The XRD patterns of (a) silica-graphenenanohybrid, (b) fsg.24, (c) fsg.48, and (d) fsg.72.

ever, there is no remarkable difference by increasing the surface modification time, which is in accordance with the FTIR results.

The X-ray diffraction patterns of silica-graphene and modified samples are shown in Fig. 5. The broad peak at around 2θ=23° can be assigned to graphene structure [39,40]. Moreover, the amorphous nature of silica aerogel shows a broad peak in the vicinity of 23° revealing an overlap spectrum. The XRD patterns show that there are no main structural changes of silica-graphene nanohybrids after treatment at different times. However, the smaller and broader peak for longer acid vapor treatment shows a little decrease in the crystalline order that might be attributed to the creation of more defect structure and functional groups emanating from longer surface modification [41].

TGA/DTG measurement of silica-graphene nanohybrid was carried out at air from room temperature to 900 °C (shown in Fig. 6). The pure silica aerogel remained stable without significant weight loss until 900 °C. It indicated the amount of graphene in the SiO_2/graphene nanohybrid was about 16 wt%, and also showed that the silica-graphene was successfully prepared via the CVD method.

Raman spectra are generally employed for the characterization of carbon nanostructure, especially graphene and its derivatives. The Raman spectra of silica-graphene nanohybrid, fsg.24, fsg.48, and fsg.72 are shown in Fig. 7. The G bands at 1,560 cm^{-1}, 1,572 cm^{-1}, 1,580 cm^{-1}, and 1,590 cm^{-1} are related to silica-graphene nanohybrid, fsg.24, fsg.48, and fsg.72, respectively. The G bands of the surface modified samples are shifted to a higher wave number due

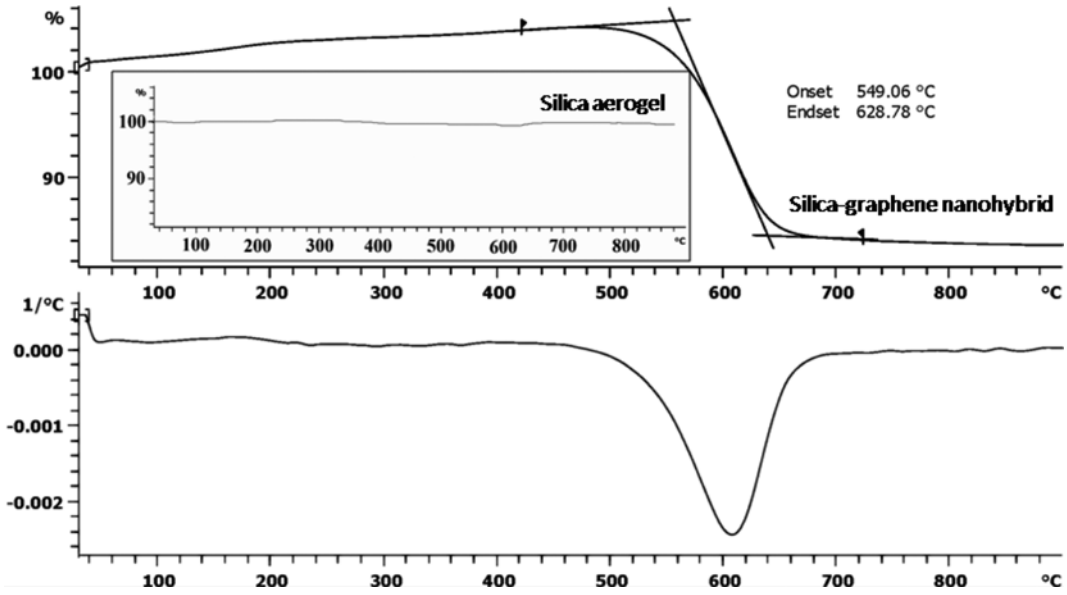

Fig. 6. TGA/DTG of silica-graphene nanohybrid. The inset shows TGA of pure silica aerogel.

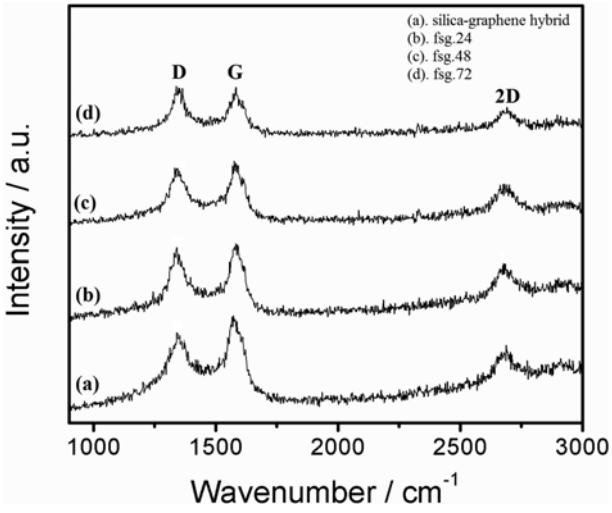

Fig. 7. Raman spectra of (a) silica-graphene nanohybrid, (b) fsg.24 (c) fsg.48,(d) fsg.72.

to the oxygenation of nanohybrid indicating the formation of sp^3 carbon atoms. The augmentation of I_D/I_G from 0.8 (silica-graphene nanohybrid) to 1.07 (fsg.72) confirms the grafting of oxygen-containing functional groups to the silica-graphene nanohybrids. Moreover, the intensity of the D band shows that defect structures have been partially created in synthesis procedure leading to increase the number of crumpled graphene layers by the passage of surface modification time. Furthermore, the relatively high intensity of 2D band around 2,600 cm^{-1} that usually appears in the monolayer graphene sheets further verifies the creation of single layer graphene [42,43]. Hence, it can be concluded that the silica-graphene nanohybrids simultaneously contain a combination of single and few layer stacked graphene sheets. The intensity ratio between the 2D and G bands ($I_{2D}/I_G \approx 0.1$) and the full width at half maximum (FWHM) of the 2D band (≈65 cm^{-1}), which are directly assigned to the number of graphene sheets, do not show any significant change with acid vapor treatment for all of the surface modified nanohybrids.

As shown in Fig. 8, the morphology of silica-graphene nanohybrid, fsg.24, fsg.48, and fsg.72 was characterized by TEM. The TEM image of silica-graphene nanohybrid (Fig. 8(a)) shows spherical silica aerogel nanoparticles (inset) and the synthesized graphene sheets on the silica catalyst. As can be seen, the graphene sheets were successfully formed on uniform silica aerogel nanoparticles by CVD method. According to TEM images, the graphene sheets get more wrinkled by increasing the time, due to the higher degree of oxidation, which can be related to more exposure of the nanohybrid to acid vapor.

STEM images of the pristine and surface modified silica-graphene nanohybrid are shown in Fig. 9. The formation of graphene sheets on silica aerogel nanoparticles was further verified (Fig. 9(a)-(d)). According to these images, the presence of both silica and graphene can be distinguished owing to the high transparency of the graphene sheets, and the few layer graphene can be observed, which is in good agreement with TEM and Raman analysis.

The zeta potentials of all samples in aqueous phase are shown in Fig. 10. The zeta potential plays an important role in determining the stability of colloidal dispersions. The zeta potential can be used as a quantitative index for investigation of stable dispersion because of inter-particle electrostatic repulsion [44]. The zeta potential of a stable emulsion can be more positive than +30 mV or more negative than −30 mV. The values of zeta potential of silica-graphene nanohybrids, fsg.24, fsg.48, and fsg.72 were obtained to be about −20.9, −33.5, −37.2, and −39.3 (mV), respectively. These results showed that increasing the time of surface modification leads to increasing the amount of zeta potential due to more oxidation duration which enhances the modification process. The more exposure to the vapor of acidic mixture indicated the higher amount of zeta potential and more stability in aqueous dispersions.

Fig. 11(a)-(i) depicts the microscopy images of the emulsions

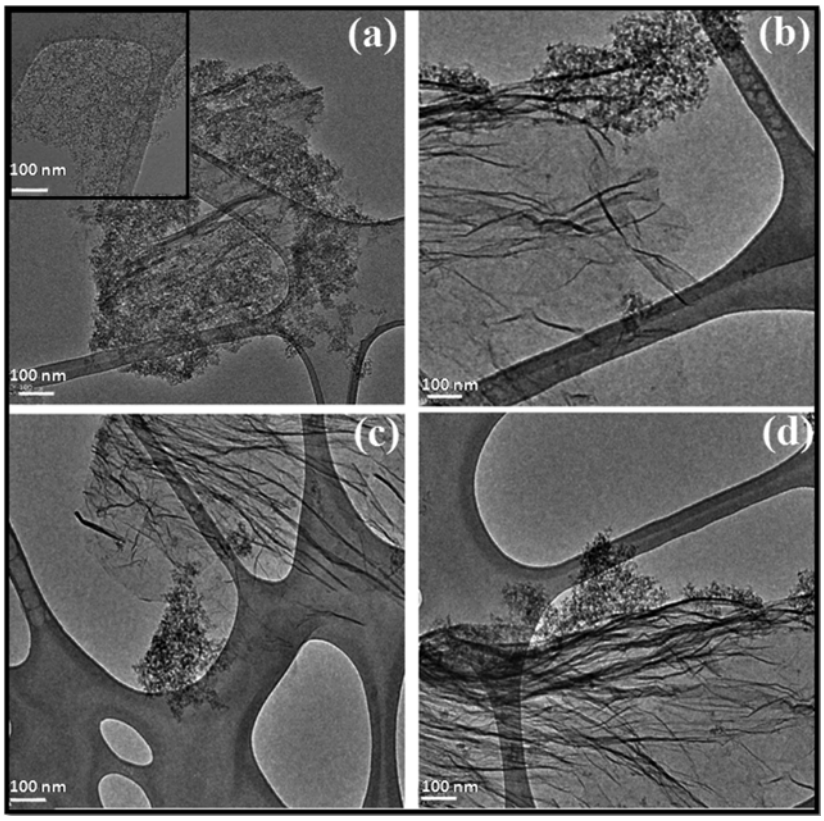

Fig. 8. TEM images of (a) silica-graphene nanohybrids, silica aerogel (inset) (b) fsg.24, (c) fsg.48, (d) fsg.72.

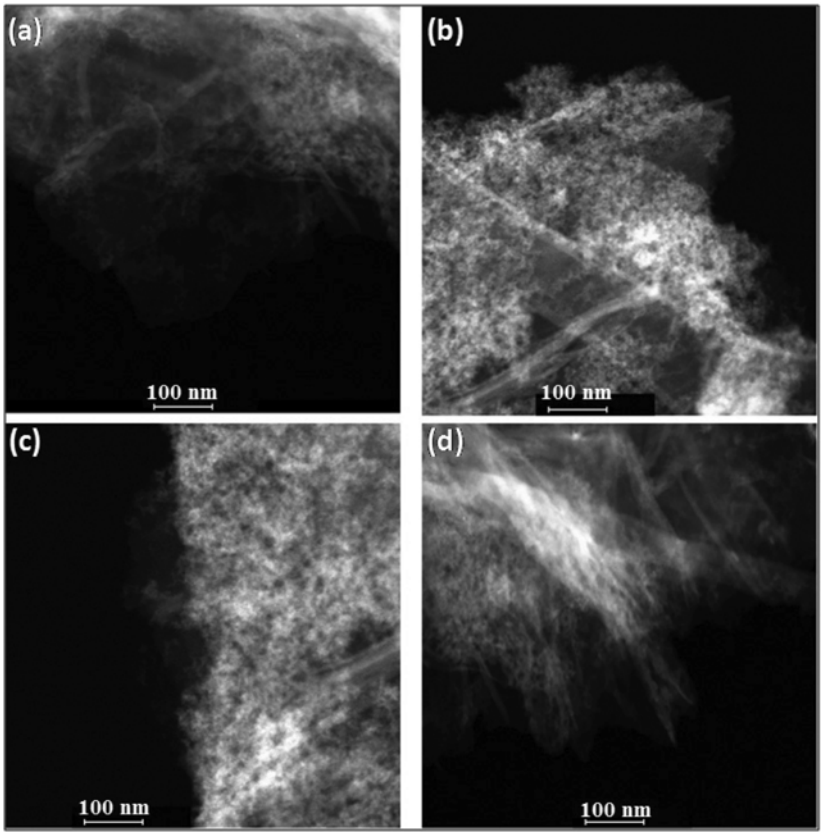

Fig. 9. STEM images of (a) silica-graphene nanohybrids, (b) fsg.24, (c) fsg.48, (d) fsg.72.

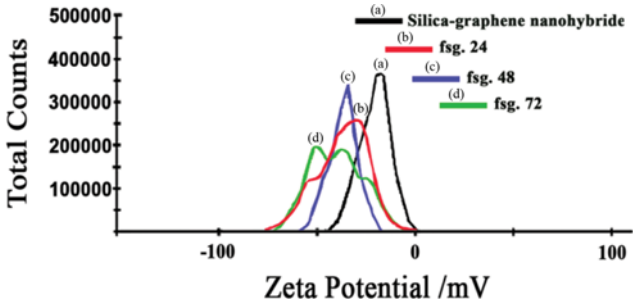

Fig. 10. The zeta Potential of (a) silica-graphene nanohybrids, (b) fsg.24, (c) fsg.48, and (d) fsg.72.

prepared by modified nanohybrids at different concentrations, while keeping water/decalin ratio to be 1 : 1. During the emulsion preparation, the nanoparticles migrate from the aqueous phase toward the oil-water interface, which prevents enlarging kinetic energy barrier [45]. In standard Pickering emulsions, the initial dispersion of particles in aqueous phase can considerably affect both the emulsion stability and droplet size, owing to limited re-coalescence during emulsification at higher particle content that can migrate to the emulsion interface [46,47]. Promoting droplet stability and also reducing the oil-water interfacial tension (IFT) occurred by migration of the particles from the dispersed phase to the oil-water interface [2,48]. Thus, a reduction in the free energy occurs while a part of the liquid-liquid interface is replaced with a

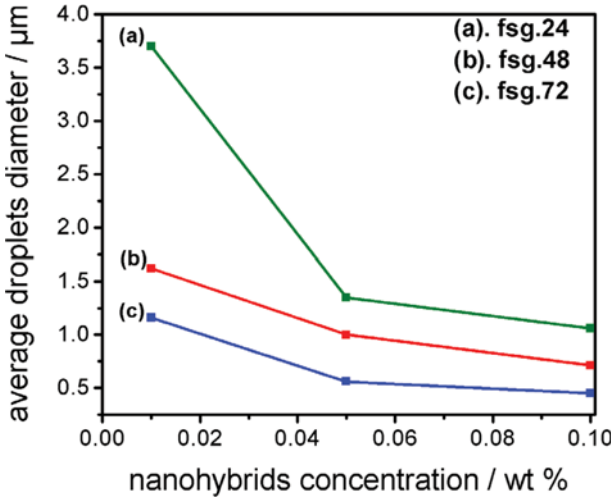

Fig. 12. Average droplets diameter as a function of surface modified nanohybrids concentration.

liquid-particle interface [49-51]. Therefore, regarding the values of zeta Potential, the formation of smaller droplets in emulsion of fsg.72 and also at the highest concentration (0.1 wt%) is more probable than other emulsions.

Therefore, as can be seen in Fig. 11(a)-(i), the size of emulsion droplets decreases with increasing functional groups in nanohy-

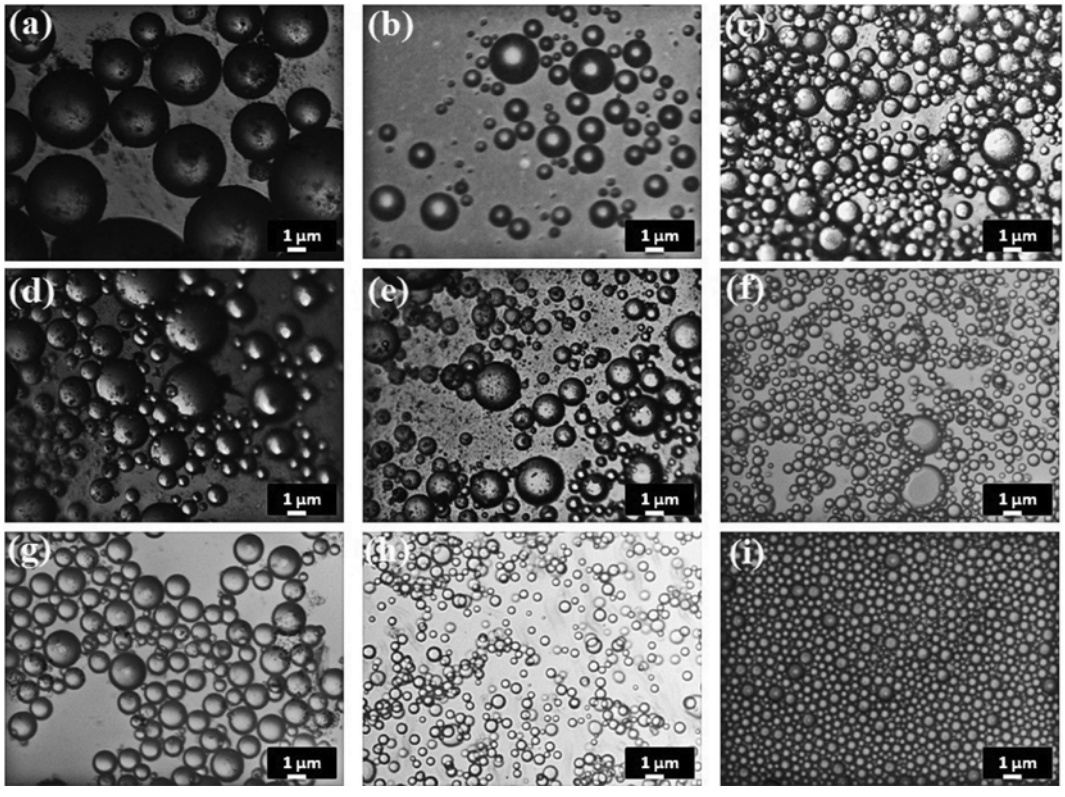

Fig. 11. The microscopy images of the emulsions at different concentrations of surface modified nanohybrid: (a) fsg.24 (0.01 wt%), (b) fsg.24 (0.05 wt%), (c) fsg.24 (0.1 wt%), (d) fsg.48 (0.01 wt%), (e) fsg.48 (0.05 wt%), (f) fsg.48 (0.1 wt%), (g) fsg.72 (0.01 wt%), (h) fsg.72 (0.05 wt%), (i) fsg.72 (0.1 wt%), oil/water ratio: 1 : 1.

brids due to migration of nanoparticles toward the oil-water interface. The average droplet diameter of each emulsion was estimated based on the microscopy images by measuring approximately 50 droplets in every image in a random order and showing as a function of nanohybrids concentration in Fig. 12. As expected, the average droplet size decreased as the nanohybrids concentration increased. The average and standard deviations droplets diameter of data at concentration of 0.1 wt% of nanohybrids show that they

Table 2. The average and standard deviation droplets diameter of emulsions at concentration of 0.1 wt%

Sample	Average droplets diameter/μm	Standard deviation/μm
Emulsion of fsg.24	1.06	0.34
Emulsion of fsg.48	0.71	0.25
Emulsion of fsg.72	0.45	0.11

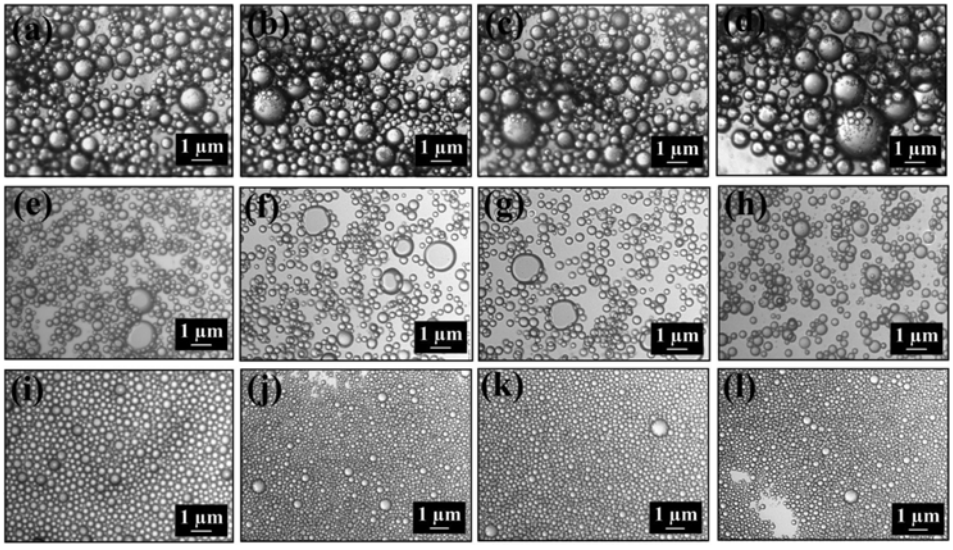

Fig. 13. The microscopy images of the emulsions stabilized by surface modified nanohybrids at different time span: (a) 0 (immediately after emulsion preparation), (b) 48, (c) 96, (d) 144 h for fsg.24, (e) 0, (f) 48, (g) 96, (h) 144 h for fsg.48, (i) 0, (j) 48, (k) 96, (l) 144 h for fsg.72 at constant concentration of 0.1 wt%.

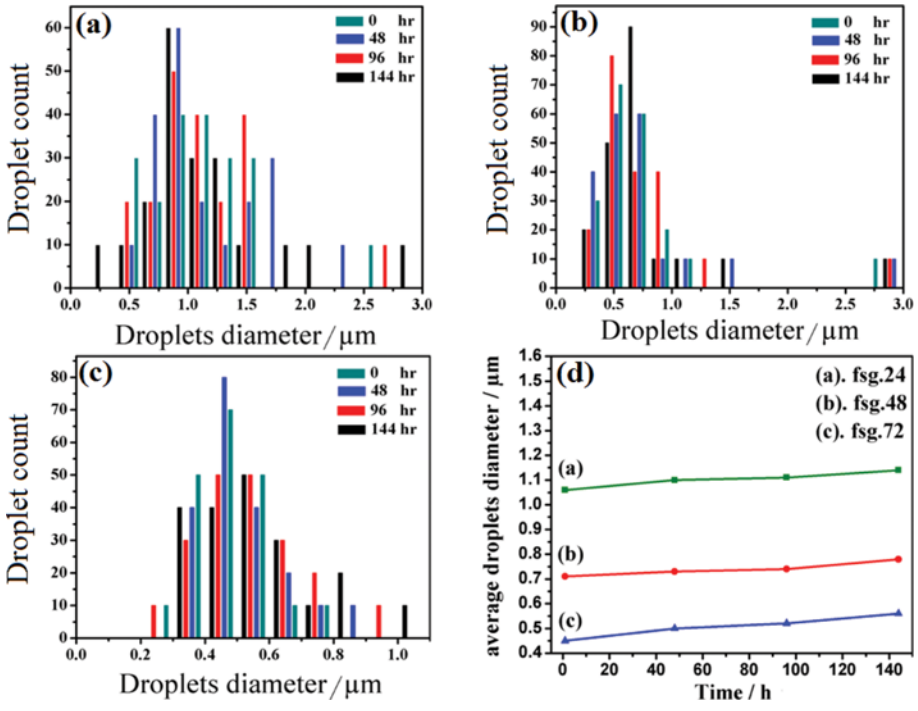

Fig. 14. Histograms of the droplet size distribution as a function of time: (a) fsg.24, (b) fsg.48, (c) fsg.72, and (d) average droplets diameter as a function of observation time (concentration of surface modified nanohybrids=0.1 wt%).

are clustered closely around the mean and have a relatively homogeneous distribution (Table 2).

To investigate the stability of the emulsions, they were kept at room temperature for six days. Following the previously established procedures in the literature [52-54], by the optical microscopy method, the emulsions were characterized during different time ranges. To have more exact studies, and our experience in the area of the nanohybrid concentration effect on the average size of droplets, a concentration of 0.1 wt% of modified nanohybrids was selected to perform these experiments. Over a period of observation time, if there are no clear changes in droplet size distribution and average droplets diameter, it can be concluded that the emulsions are stable.

Fig. 13(a)-(*l*) and Fig. 14(a)-(c) display the microscopy images of emulsions at different times with their corresponding droplet size distribution plots, respectively. As can be seen in Fig. 14(a)-(c), a shift towards a broader droplet size distribution was observed via changing the time from 0 to 144 h in all emulsions, while there was no significant change in droplet size. Therefore, the present observations are relatively convincing proofs showing the surface modified silica-graphene nanohybrids adsorbed at the oil-water interface, and they occupied a large interfacial area to hinder droplets coalescence [25,55]. As a matter of fact, during the adsorption of nanoparticles on the interface, some rigid shells are formed and lead to the electrostatic repulsions and steric hindrance; therefore, it can be considered as a reason for the stability of emulsions by the modified silica-graphene [56,57]. On the other hand, there is no considerable change in the average droplets diameter over a period of storage time (Fig. 14(d)), implying the high stability of emulsions.

To investigate the individual and particular behavior of emulsion in both deionized water and decalin, an equal amount of emulsion was dropped in a constant volume of deionized water and decalin. It was generally observed that when a drop of oil-in-water emulsion is dispersed in water, the added drop remains unchanged in oil. By addition of a drop of the as-prepared emulsions to water and decalin, it was also found that the type of emulsions could be considered as decalin in water (see Fig. 15 as an example) [58].

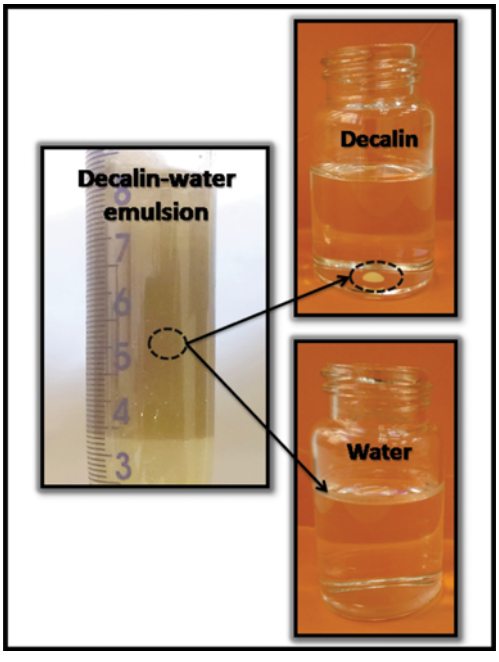

Fig. 15. The behavior of an added droplet of emulsion in deionized water and decalin.

CONCLUSION

Silica-graphene nanohybrid was prepared via CVD method and then modified by using a mixture nitric and sulfuric acid vapors as a new approach. The amount of graphene in the nanohybrid was estimated to be about 16 wt% according to TGA analysis. The modified nanohybrids demonstrated excellent stabilization in aqueous phase, which was efficiently used for preparing the stable oil-water emulsions. The values of zeta potential of nanohybrids were more negative than –30 mV, confirming the high stability of nanohybrids in water. The surface modification process was carried out in different time. According to the FT-IR, XPS and the values of zeta potential, the structural defects, the oxygen containing functional groups, and consequently the stability of nanohybrids in water have increased by increasing the modification time. The value of zeta potential and the minimum average droplets diameter of emulsion were directly dependent on the time of chemically surface modification and the concentration of nanohybrids. This work showed that hybridization and surface modification of graphene would remarkably enhance the stability of Pickering emulsions.

REFERENCES

1. S. Crossley, J. Faria, M. Shen and D. E. Resasco, *Science*, **327**, 68 (2010).
2. S. Ma, Y. Wang, K. Jiang and X. Han, *Nano Res.*, **8**, 2603 (2015).
3. E. Dickinson, *Curr. Opin. Colloid Interface Sci.*, **15**, 40 (2010).
4. M. Rayner, A. Timgren, M. Sjöö and P. Dejmek, *J. Sci. Food Agric.*, **92**, 1841 (2012).
5. D. Marku, M. Wahlgren, M. Rayner, M. Sjöö and A. Timgren, *Int. J. Pharm.*, **428**, 1 (2012).
6. F. Leal-Calderon and V. Schmitt, *Curr. Opin. Colloid Interface Sci.*, **13**, 217 (2008).
7. S. Melle, M. Lask and G. G. Fuller, *Langmuir*, **21**, 2158 (2005).
8. L. Torres, R. Iturbe, M. Snowden, B. Chowdhry and S. Leharne, *Colloids Surf., A Physicochem. Eng. Asp.*, **302**, 439 (2007).
9. B. Binks and S. Lumsdon, *Langmuir*, **16**, 8622 (2000).
10. A. Schrade, K. Landfester and U. Ziener, *Chem. Soc. Rev.*, **42**, 6823 (2013).
11. J. Shi, X. Wang, W. Zhang, Z. Jiang, Y. Liang, Y. Zhu and C. Zhang, *Adv. Funct. Mater.*, **23**, 1450 (2013).
12. C. Wu, S. Bai, M. B. Ansorge-Schumacher and D. Wang, *Adv. Mater.*, **23**, 5694 (2011).
13. J. Zhou, X. Qiao, B. P. Binks, K. Sun, M. Bai, Y. Li and Y. Liu, *Langmuir*, **27**, 3308 (2011).
14. T. Chen, P. J. Colver and S. A. Bon, *Adv. Mater.*, **19**, 2286 (2007).
15. X.-C. Luu, J. Yu and A. Striolo, *Langmuir*, **29**, 7221 (2013).
16. M. Shen and D. E. Resasco, *Langmuir*, **25**, 10843 (2009).
17. B. P. Binks and J. A. Rodrigues, *Angew. Chem.*, **117**, 445 (2005).
18. Y. Cui, M. Threlfall and J. S. van Duijneveldt, *J. Colloid Interface*

Sci., **356**, 665 (2011).
19. C. C. Berton-Carabin and K. Schroën, *Annu. Rev. Food Sci. Technol.*, **6**, 263 (2015).
20. D. Chen, H. Zhang, Y. Liu and J. Li, *Energy Environ. Sci.*, **6**, 1362 (2013).
21. A. Yadegari, M. Omidi, M. Choolaei, F. Haghiralsadat and F. Yazdian, *Procedia Eng.*, **87**, 967 (2014).
22. A. Yadegari, M. Omidi, F. Yazdian, H. Zali and L. Tayebi, *RSC Adv.*, **7**, 2365 (2017).
23. M. Omidi, A. Fathinia, M. Farahani, Z. Niknam, A. Yadegari, M. Hashemi, H. Jazayeri, H. Zali, M. Zahedinik and L. Tayebi, *Advanced 2D Materials*, 433 (2016).
24. M. Hashemi, A. Yadegari, G. Yazdanpanah, S. Jabbehdari, M. Omidi and L. Tayebi, *RSC Adv.*, **6**, 74072 (2016).
25. J. Kim, L. J. Cote, F. Kim, W. Yuan, K. R. Shull and J. Huang, *J. Am. Chem. Soc.*, **132**, 8180 (2010).
26. X. Song, Y. Yang, J. Liu and H. Zhao, *Langmuir*, **27**, 1186 (2010).
27. F. Hoffmann, M. Cornelius, J. Morell and M. Fröba, *Angew. Chem. Int. Ed.*, **45**, 3216 (2006).
28. V. O. Ikem, A. Menner and A. Bismarck, *Angew. Chem. Int. Ed.*, **47**, 8277 (2008).
29. M. Choolaei, A. M. Rashidi, M. Ardjmand, A. Yadegari and H. Soltanian, *Mater. Sci. Eng. A*, **538**, 288 (2012).
30. D. R. Dreyer, S. Park, C. W. Bielawski and R. S. Ruoff, *Chem. Soc. Rev.*, **39**, 228 (2010).
31. Y. Wen, H. Ding and Y. Shan, *Nanoscale*, **3**, 4411 (2011).
32. J. Simmons, B. Nichols, S. Baker, M. S. Marcus, O. Castellini, C.-S. Lee, R. Hamers and M. Eriksson, *J. Phys. Chem. B*, **110**, 7113 (2006).
33. J. Zhao, A. Buldum, J. Han and J. P. Lu, *Nanotechnology*, **13**, 195 (2002).
34. G. Ovejero, J. Sotelo, M. Romero, A. Rodríguez, M. Ocana, G. Rodríguez and J. Garcia, *Ind. Eng. Chem. Res.*, **45**, 2206 (2006).
35. S. Santangelo, G. Messina, G. Faggio, S. Abdul Rahim and C. Milone, *J. Raman Spectrosc.*, **43**, 1432 (2012).
36. X. Niu, W. Yang, H. Guo, J. Ren and J. Gao, *Biosens. Bioelectron.*, **41**, 225 (2013).
37. W. Xia, C. Jin, S. Kundu and M. Muhler, *Carbon*, **47**, 919 (2009).
38. U. K. Bangi, S. L. Dhere and A. V. Rao, *J. Mater. Sci.*, **45**, 2944 (2010).
39. T. Chen, F. Deng, J. Zhu, C. Chen, G. Sun, S. Ma and X. Yang, *J. Mater. Chem.*, **22**, 15190 (2012).
40. Y. Luo, D. Kong, Y. Jia, J. Luo, Y. Lu, D. Zhang, K. Qiu, C. M. Li and T. Yu, *RSC Adv.*, **3**, 5851 (2013).
41. K. Krishnamoorthy, M. Veerapandian, K. Yun and S.-J. Kim, *Carbon*, **53**, 38 (2013).
42. O.-K. Park, S. Lee, H.-I. Joh, J. K. Kim, P.-H. Kang, J. H. Lee and B.-C. Ku, *Polymer*, **53**, 2168 (2012).
43. A. Ferrari, J. Meyer, V. Scardaci, C. Casiraghi, M. Lazzeri, F. Mauri, S. Piscanec, D. Jiang, K. Novoselov and S. Roth, *Phys. Rev. Lett.*, **97**, 187401 (2006).
44. L. Jiang, L. Gao and J. Sun, *J. Colloid Interface Sci.*, **260**, 89 (2003).
45. Z.-G. Cui, C.-F. Cui, Y. Zhu and B. Binks, *Langmuir*, **28**, 314 (2011).
46. B. Binks and S. Lumsdon, *Langmuir*, **17**, 4540 (2001).
47. Y. Chevalier and M.-A. Bolzinger, *Colloids Surf., A Physicochem. Eng. Asp.*, **439**, 23 (2013).
48. N. Nikfarjam, N. T. Qazvini and Y. Deng, *Colloid Polym. Sci.*, **292**, 599 (2014).
49. S. A. Bon and P. J. Colver, *Langmuir*, **23**, 8316 (2007).
50. H. J. Yang, W. G. Cho and S. N. Park, *Ind. Eng. Chem.*, **15**, 331 (2009).
51. M. M. Gudarzi and F. Sharif, *Soft Matter*, **7**, 3432 (2011).
52. A. G. Cunha, J.-B. Mougel, B. Cathala, L. A. Berglund and I. Capron, *Langmuir*, **30**, 9327 (2014).
53. H. Yan, B. Zhao, Y. Long, L. Zheng, C.-H. Tung and K. Song, *Colloids Surf., A Physicochem. Eng. Asp.*, **482**, 639 (2015).
54. L. Ridel, M.-A. Bolzinger, N. Gilon-Delepine, P.-Y. Dugas and Y. Chevalier, *Soft Matter*, **12**, 7564 (2016).
55. F. Kim, L. J. Cote and J. Huang, *Adv. Mater.*, **22**, 1954 (2010).
56. P. Guo, H. Song and X. Chen, *J. Mater. Chem.*, **20**, 4867 (2010).
57. H. A. Wege, S. Kim, V. N. Paunov, Q. Zhong and O. D. Velev, *Langmuir*, **24**, 9245 (2008).
58. N. Ashby and B. Binks, *Phys. Chem. Chem. Phys.*, **2**, 5640 (2000).